Published in "Bioconjugate Chemistry 26(12): 2408–2418, 2015"
which should be cited to refer to this work.

Synthesis of FMRFaNV, a Photoreleasable Caged Transmitter Designed to Study Neuron–Glia Interactions in the Central Nervous System

Elia Janett,[†] Yann Bernardinelli,[‡] Dominique Müller,[‡,#] and Christian G. Bochet*[,†]

[†]Department of Chemistry, University of Fribourg, Chemin du Musée 9, CH-1700 Fribourg, Switzerland
[‡]Department of Basic Neurosciences, School of Medicine, University of Geneva, rue Michel-Servet 1, CH-1211 Geneva 4, Switzerland

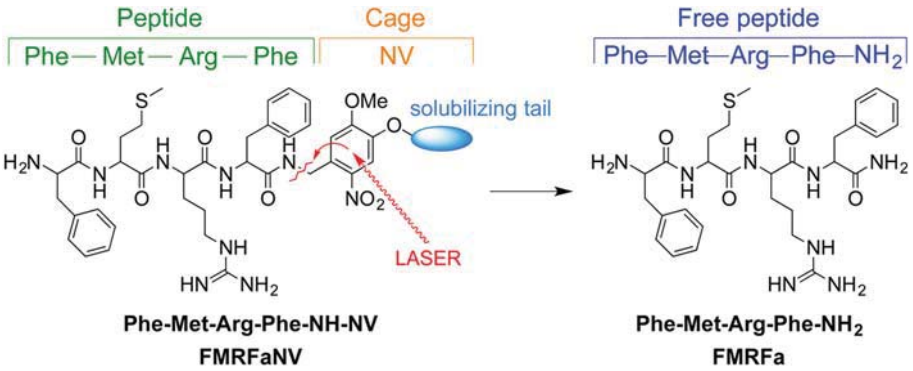

ABSTRACT: Neuroscience studies require technologies able to deliver compounds with both scale and timing compatibility with morphological and physiological synaptic properties. In this light, two-photon flash photolysis has been extensively used to successfully apply glutamate or other neurotransmitters at the synaptic level. However, the set of commercially available caged compounds is restricted and incompatible with studies demanding high cell specificity. The gain in cell specificity is especially relevant and challenging when studying neuron–glia interactions in the central nervous system. Here we develop a system to mimic the metabotropic glutamate receptor-dependent response of astrocytes, a glial cell type, following synaptic glutamate release. For this, we expressed an exogeneous orphan Gq-coupled protein of the *Mas-related-gene* (Mrg) family in glial cells and generated an MrgR's agonist peptide (FMRFa) that was chemically caged with a nitroveratryl photolabile protecting group (NV). NV has an appropriate quantum yield and a high absorption maximum that makes it very adapted to experiments with very short irradiation time. This novel caged compound allowed the activation of MrgR with both single- and two-photon light sources. Indeed, MrgR activation induced calcium transients and morphological changes in astrocytes as described previously. Thus, FMRFaNV is a very promising tool to study neuron–glia interactions.

INTRODUCTION

The human brain is formed of two main classes of neural cells: neurons and glia. Even if neurons are more studied, because of their important role in the transmission and management of information, glial cells appear to be as crucial as neurons for proper brain functioning. Glial cells are principally responsible to support neurons, furnishing them physical support, nutrients, insulation, and protection.[1] Among glial cell types, astrocytes are the most intriguing as they can actively support synaptic function and structure in many ways.[2] They control the amount of glutamate—the most common neurotransmitter—by taking it up from the synaptic cleft,[3] they furnish lactate[4] as energetic substrate to the neurons,[5] and regulate the osmotic gradients and the homeostasis.[6]

Until recently, neurons were considered the only actor in neurotransmission. Nowadays there is evidence that astrocytes participate in information processing in the brain and that they are able to send signals to neurons, thanks to the presence of many cellular processes—that give them a star-shaped aspect—and their position in the periphery of synapses.[7] Perisynaptic astrocytic processes (PAP) participate to the synaptic transmission by either taking up neurotranmistters or sending gliotransmitters.[8]

Despite evidence for the role of astrocytes in the regulation of synaptic activity and plasticity, the mechanisms of these effects is still highly debated.[9] These controversies are mostly due to technical challenges when studying neuron–glia interactions. Indeed, pre- and post-synaptic neuronal components share common neurotransmitter receptors with PAP, rendering particularly difficult to dissociate cellular responses pharmacologically.

To encompass this issue, genetically modified astrocytes expressing foreign receptors can be used to specifically activate them. However, the delivery of agonists with spatial and temporal resolution compatible with synaptic properties is limiting the interpretation of the aforementioned approaches. Novel techniques, such as optogenetics, seem to be hardly applicable when activating small cellular structure,[10] and do not reflect agonist binding to receptors. Consequently, two-photon flash photolysis is the technique of choice for such experimental paradigm.

Here, we used a previously described approach to trigger intracellular calcium (a key component of neuron−glia interaction mechanisms) specifically in astrocytes with the exogenous Mas-Related-Gene Gq coupled receptor (MrgA1R).[11] We further developed this approach by performing specific viral gene delivery in astrocytes and synthesized the MrgA1 agonist peptide in a photocleavable version compatible with two-photon flash photolysis. We describe here the synthesis and the properties of this photocleavable compound which allowed to specifically, spatially, and temporally activate PAP in the synapse periphery.

RESULTS AND DISCUSSION

Astrocytes possess well-accepted calcium excitability in response to neurotransmitters.[12] Astrocytic calcium elevations (ACE) are central in the mechanism of their interactions with neurons. At glutamatergic synapses, ACE are induced through glutamate binding to type 1 metabotrobic glutamate receptors 1 and 5 (mGluR).[13] mGluR are Gq-coupled receptors leading to the release of calcium from the internal stores. To mimic glutamate-dependent ACE, others have used transgenic mice line expressing a foreigner Gq-coupled protein of the Mas-related-gene family (Mrg) under the astrocytic promoter Glial Fibrillary Acidic Protein (GFAP). The small peptide FMRFa being agonist of MrgA1 and possessing no endogenous receptor in the CNS, it was used to specifically induce ACE in MrgA1 expressing astrocytes.[11] Here, we produced Semliki Forest Viruses (SFV) to drive the gene of MrgA1R together with a fluorescent protein. To specifically address SFV in astrocytes, we took advantage of the A7-SFV strains that preferentially infect astrocytes.[14] A7-SFV driving the gene of MrgA1 tagged with MycHis and the fluorescent protein mCherryf targeted to the plasma membrane through farnesylation (Figure 1A), were injected in the stratum radiatum of the CA1 region of hippocampus (Figure 1A). As described previously, SFV A7 infects several glial cell types.[15] Immunostaining against GFAP showed that infected cells having a very complex shape made of thousands of thin fillopodia-like structures were positive for astrocytic markers GFAP and S100B (Figure 1B). Importantly, mCherryf positive astrocytes were also expressing MrgA1 protein as demonstrated by immunoreaction against MycHis (Figure 1C). Organotypic hippocampal slices were then bulk-loaded with a cell-permeant calcium sensitive dye (Fluo-8) that preferentially loads into astrocytes. When MrgA1 agonist FMRFa (Scheme 1, 15 μM) was bath applied, MrgA1 positive astrocytes were significantly and specifically elevating their intracellular calcium (Figure 1D).

To test the influence of the astrocytic activation in spatially defined domains, the use of a caged-FMRFa neurotransmitter was proposed (Scheme 1).[16] Its activation must be controllable at a single PAP level. Thus, a photocleavable cage was chosen, which can be removed by flash photolysis allowing a precise spatial control. The nitroveratryl photolabile protecting group (NV) has an appropriate quantum yield and a high absorption maximum that makes it very adapted to in vivo studies and experiments with very short irradiation time.[17] Some drawbacks

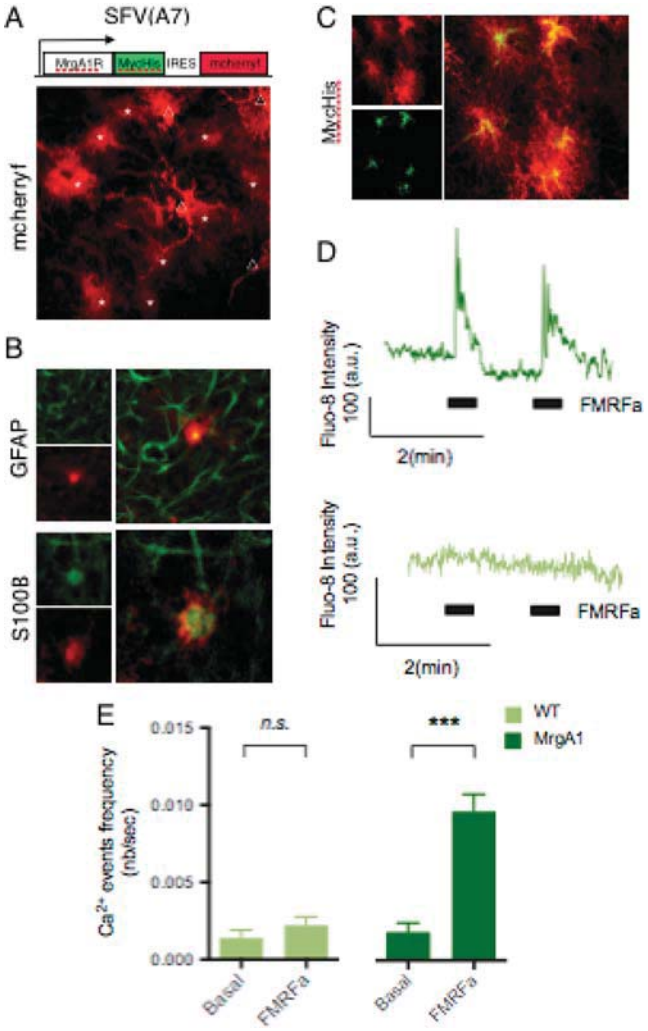

Figure 1. Exogeneous Gq coupled receptors to specifically activate astrocytes. (A) Scheme of the viral DNA. SFV A7 drives the gene of MrgA1R (white) with MycHis tag (green). The red fluorescent protein mCherry (red) is expressed bicistronically using an IRES sequence. *Z*-stack projection of confocal images illustrating a majority of infected astrocytes (*) and other glial-cells (Δ) both expressing mCherryf. (B) Immunostaining images showing that SFV A7 principally infect astrocytes. The astrocytic marker GFAP (top picture, green) colocalized with infected astrocytes (red). The astrocytic marker S100B (bottom picture, green), also colocalized with infected cells (red). (C) Immunostaining against MycHis (green) demonstrating that astrocytes expressing mCherry (red) are also expressing MrgA1. (D) Representative trace of the calcium-sensitive dye Fluo-8 fluorescence intensity plotted against time. When MrgA1 agonist FMRFa was superfused on infected astrocytes (MrgA1, dark green), Fluo-8 signal intensity increased. No changes of fluorescence were observed in noninfected cells (light green, WT). (E) Quantification of calcium signals before and during bath application of FMRFa in MrgA1 expressing- and WT-astrocytes.

(such as the formation of side products and the necessity of synthetic transformation for particular tailoring) are offset by a robustness in the photolysis in a large variety of conditions, including organic or aqueous solvents, and without particular care for the presence of oxygen. Moreover its ability to be coupled to a carboxylic acid, but liberating an amide function after photolysis, facilitates the synthesis from the readily available FMRF−OH tetrapeptide (Scheme 2).

Scheme 1. FMRFa

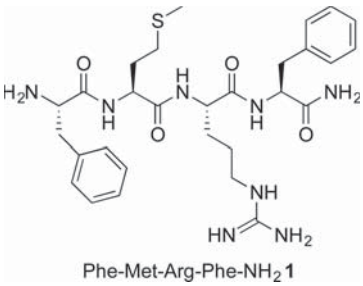

Scheme 2. Synthesis and Photolysis Pathway

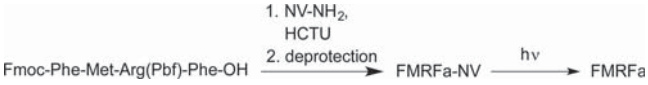

Cell cultures could thus be incubated with the protected inactive peptide, without induction of the signalization, and caged FMRFa should then be very precisely locally activated by the use of a laser. Interaction of the free neurotransmitter with the receptor MrGA1 will induce the subsequent activation of the irradiated cell and of all the cells interacting with it. The signalization cascade will be followed by observation of the Ca^{2+}-induced fluorescence emission of the active cells.[11]

The tetrapeptide was synthesized with an automated peptide synthesizer on solid phase, using a chlorotrityl resin and Fmoc protected amino acids; the coupling steps were performed using HCTU. The arginine amino acid was protected with a 2,2,4,6,7-pentamethyldihydrobenzofuran-5-sulfonyl (Pbf) group to avoid side reactions on the guanidine function. Deprotection from the resin was achieved with a solution of TFA in trifluoroethanol and CH_2Cl_2 (1:1.8). The Fmoc group of the last amino acid (phenylalanine), as well as the guanidine protection, were not removed at the end of the synthesis to prevent interference during the coupling with the nitroveratrylamine cage.

The nitroveratrylamine NV-NH_2 **4** was synthesized from the commercially available and inexpensive nitroveratraldehyde **2**. As our attempts to obtain the amine from the alcohol—or corresponding leaving group—under normal amination conditions were not successful, we opted for a two-step sequence, forming and then reducing an *O*-methyl oxime group (Scheme 3).[18]

Coupling of **4** with Fmoc-Phe-Met-Arg(Pbf)-Phe-OH **5** was performed under classical peptide synthesis conditions using HCTU as coupling agent (Scheme 4). The remaining Fmoc group was immediately removed by the addition of piperidine. The final product was purified by flash chromatography on a C18 reverse-phase column. The caged peptide **6** was shown to be very sensitive to temperature. Evaporation of the solvents must be carried out at room temperature. Finally the Pbf group was removed with concentrated TFA and the crude product

Scheme 3. Synthesis of the Nitroveratrylamine 4

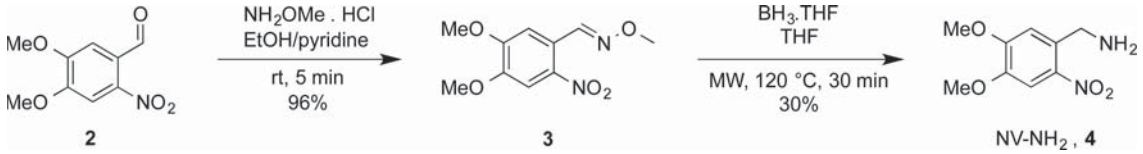

Scheme 4. Synthesis and Photolysis of the FMRFaNV 7

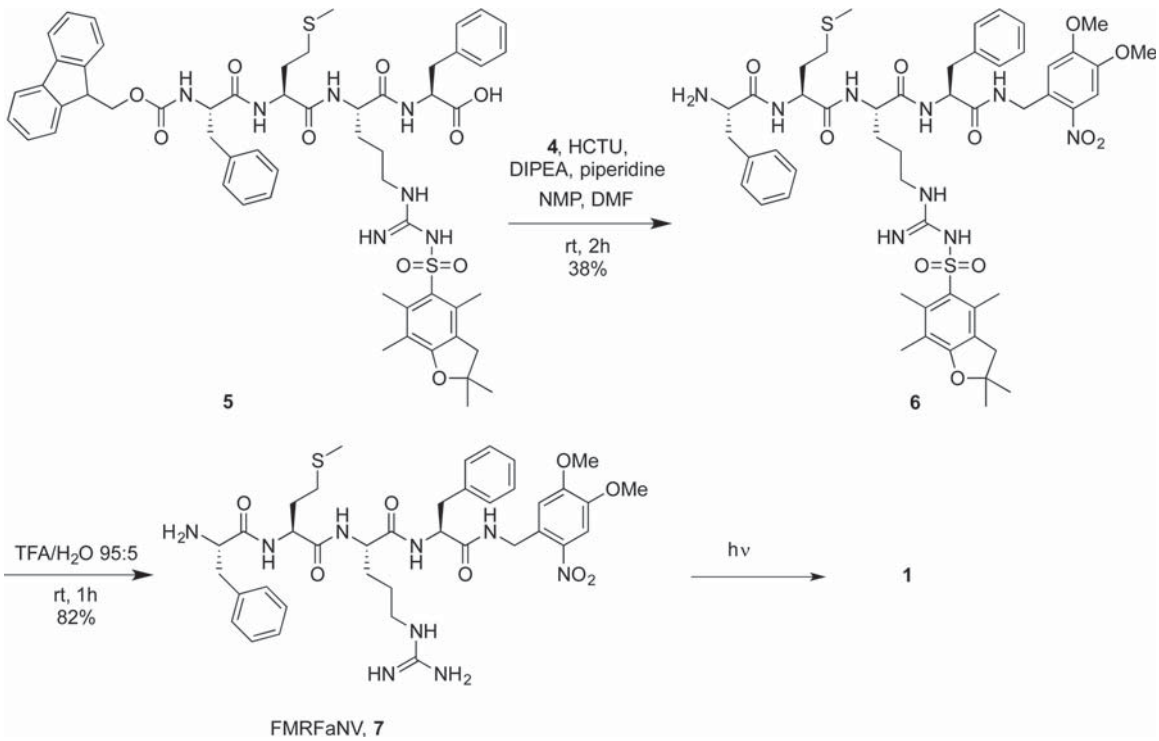

Scheme 5. Synthesis of the TEGNVNH$_2$ 16

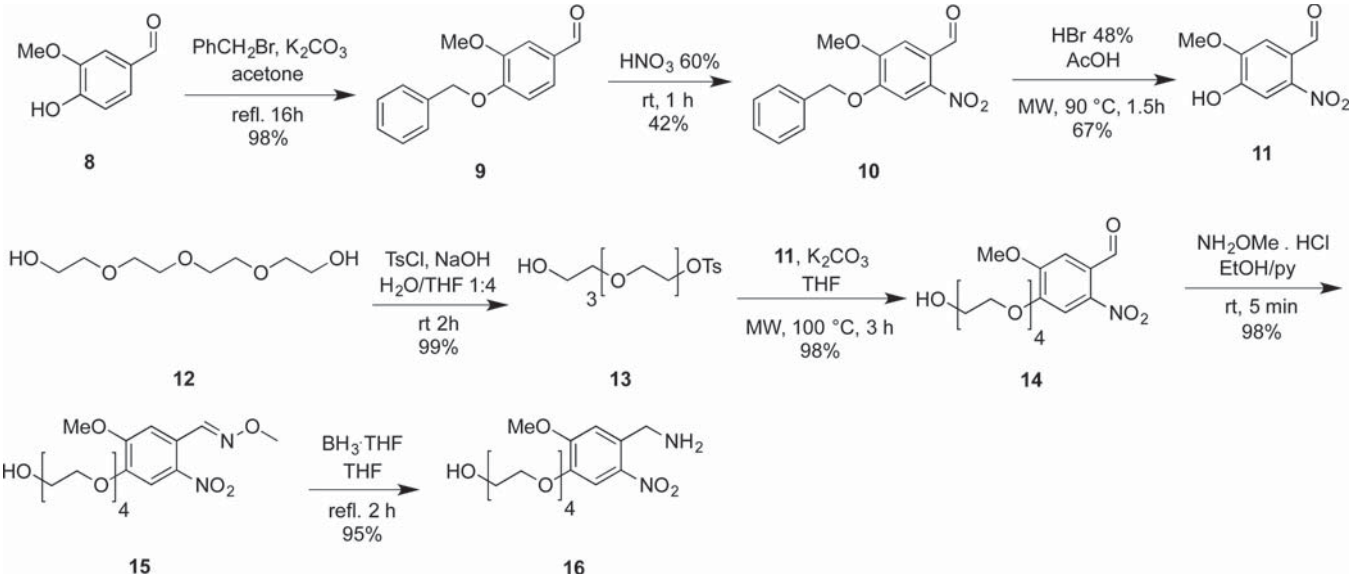

Scheme 6. Synthesis of the FMRFaNVTEG 20

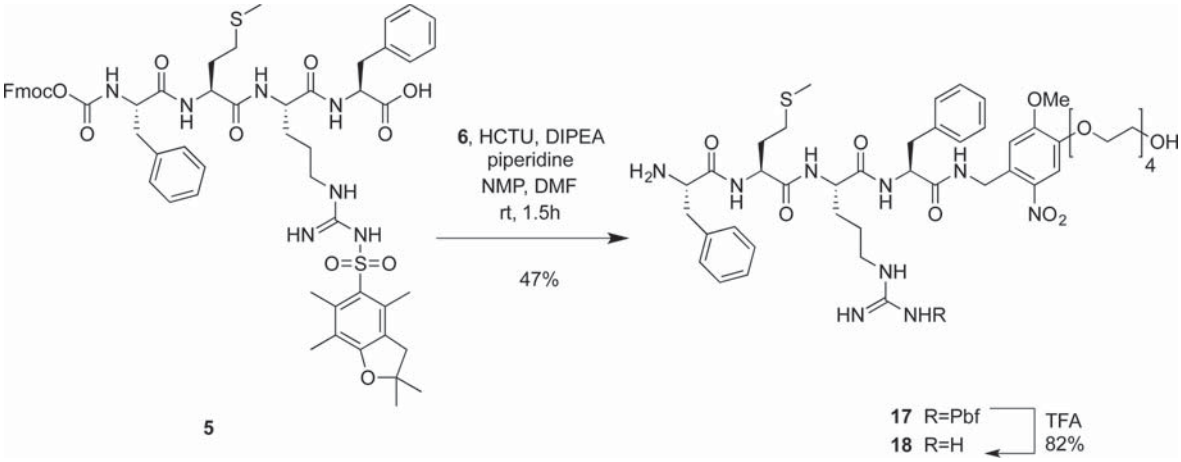

was purified again by chromatography. A photolysis test was performed using a 385 nm LED lamp. Following of the reaction by ESI-MS showed the almost complete liberation of FMRFa (Scheme 4) in 3 h.

Unfortunately, FMRFaNV **7** showed poor solubility under physiological conditions. Thus, an analogue was synthesized, bearing a more hydrophilic unit. Hence, we replaced one of the two methoxy groups of the cage with a tetraethylene glycol (TEG) function, known to increase the solubility in water.[19] The modified nitrobenzaldehyde was obtained by nitration and coupling of a TEG chain on vanillin **8** (Scheme 5). The phenolic group needed first to be protected as a benzyl ether, in order to obtain regioselectivity in the nitration,[20,16,17] before rehydrolysis with hydrobromic acid. The TEG group was monoactivated before coupling, by reaction with *p*-toluenesulfonyl chloride.[16,17] The use of a large excess of tetraethylene glycol (10 equiv) prevented the formation of the difunctionalized product. The obtained tosylate was then coupled with nitrovanillin in basic medium under microwave heating.

The desired TEGNVNH$_2$ **16** was then obtained following the procedure of oximation and reduction described above.

This compound proved to be very sensitive to air, light, and temperature. To avoid degradation, the more stable hydrochloride was obtained by extraction with HCl 1N and direct concentration of the aqueous phase under vacuum at 50 °C. The coupling of this new protecting group with the tetrapeptide was carried out in the usual manner, using HCTU (Scheme 6).

A quantum yield measurement was performed to determine the photolability of the cage. First the photon flow of the spectrometer used for the measurements was determined by an actinometry experiment with the ferrioxalate technique.[18] Then the quantum yield of the FMRFaNVTEG was calculated by irradiating a 0.4 mM solution in water for different times. The disappearance of the starting product was determined by UV/vis spectroscopy and plotted as a function of the time. The reaction rate was calculated and the obtained value was then divided by the previously measured quantum flow to give a photolysis quantum yield at 360 nm of 0.023 (a related saturated amide, lacking the TEG group was reported with a photolysis quantum yield of 0.072).[21] In a separate experiment, NMR analysis of the crude photolysis mixture (20 min at 385 nm) showed the release of the peptide, together with the TEG-containing side product,

by comparison with an authentic sample of FMRFa measured in the same experimental conditions (D_2O, see SI).

The caged FMRFaNVTEG was bath applied on the hippocampal slices. Its caged form was shown to have no influence on the activity of astrocytes (not shown), while UV flashes at 365 nm provoked calcium signals in astrocytes infected with MrgA1R (Figure 2A–D). The majority of wild type astrocytes

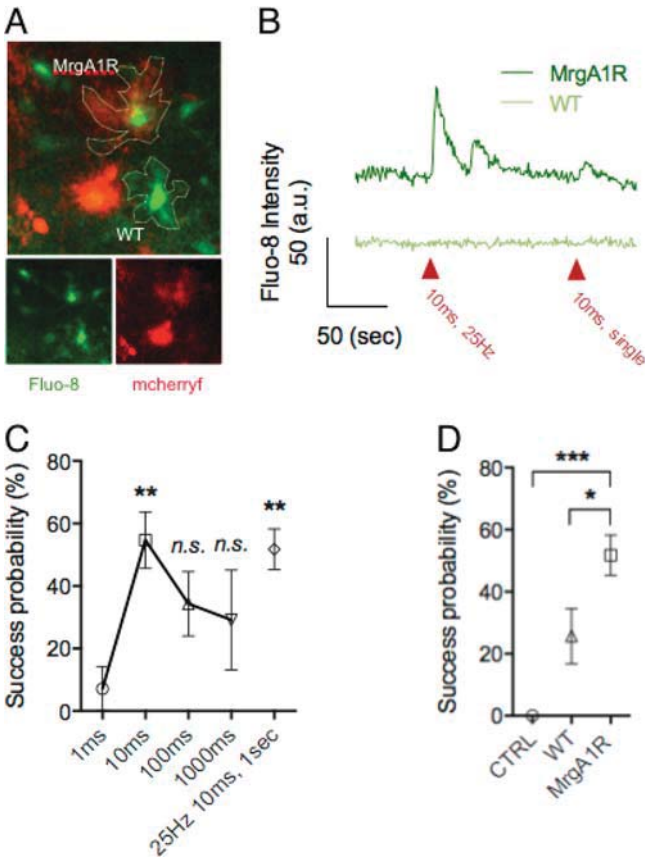

Figure 2. 365-nm uncaging of FMRFaNVTEG on MrgA1 astrocytes. (A) Single plane confocal images showing astrocytes loaded with the calcium-sensitive dye Fluo-8 (green) and expressing mCherryf (red). (B) Representative trace of Fluo-8 intensities showing that mCherryf positive astrocytes (MrgA1R) elevate their intracellular calcium following 365-nm UV flashes (red arrowhead) but not mCherryf-negative astrocytes (WT). (C) The UV flash probability of success in evoking a calcium transient was evaluated for different UV-flash length of 1 ms ($n = 14$), 10 ms ($n = 25$), 100 ms ($n = 17$), 1 s ($n = 8$), and 10 ms pulses at 25 Hz for 1 s ($n = 28$). (D) 10 ms UV flashes were pulsed at 25 Hz for 1 s and the success probability in evoking calcium events in astrocytes evaluated when FMRFa-NV was absent (CTRL, $n = 8$), in nonexpressing mCherryf astrocytes (WT, $n = 12$) and in mCherryf positive astrocytes (MrgA1R, $n = 28$). (Data are Means ± SEM, Statistics are one-way ANOVA, *n.s.* = $p > 0.05$; * = $p < 0.05$; ** = $p < 0.001$; *** = $p < 0.0001$).

(WT, e.g., noninfected) in the illuminated area failed to increase their intracellular calcium (Figure 2A,B,D). Increasing the length of UV illumination from 1 ms to 1 s showed that 10 ms of illumination is optimally evoking ACE (Figure 1C). Only about 60% of UV-flashes were evoking ACE (Figure 1C). Increasing the duration of illumination above 10 ms does not increase the success in evoking ACE nor pulsing light at 25 Hz (Figure 1C). UV flashes delivered in the absence of the caged compound failed to evoke ACE. All together, those data indicate that ACE can be successfully evoked through FMRFa-NVTEG photolysis.

Two-photon flash photolysis was then used to deliver FMRFa at the synaptic level. To evaluate the effectiveness of uncaging, the amount of movement of the astrocytic process was evaluated. Indeed, PAPs are known to be highly motile structures[14] that can dynamically move in the periphery of the synapse. This motility is believed to be dependent on neuronal activity and astrocytic mGluR.[19] Neurons were infected with a neuron-specific strain of SFV driving the gene of a green fluorescent protein (GFP), while astrocytes were infected with SFVA7MrgA1R mCherryf (Figure 3A). Repetitive imaging of the neuronal spine and astrocytic process contacts showed that the processes are highly motile (Figure 1B). Movement could be quantified by using an index of motility (MI) as described previously (Figure 1C).[19] While recording MI for two consecutive 10 min period, MI stayed stable (Figure 1D). A 725-nm two-photon light beam sent at a single point (8 × 1 ms at 1 Hz ref) between neuronal and astrocytic membrane resulted in an increase of MI when FMRFaNVTEG was present and did not evoked MI increase when astrocytes were lacking MrgA1R (Figure 1D). This indicates that FMRFaNV-TEG can be reliably used for 2P uncaging with a synaptic resolution.

CONCLUSION

Our synthesis of a photolabile caged neurotransmitter allowed the study of the interaction between cellular actors at a very precise spatial domain, with a fully temporal control. The chosen photocleavable protecting group revealed to be very adapted to flash photolysis experiments. We also demonstrated the possibility to increase the solubility of the protected substrate by adding hydrophilic chains on the photolabile group, without inhibiting the photolytic release of the biomolecule. The final synthetic procedure is simple and quite flexible and it should be seemingly applicable to many other biologically active molecules involved in cell signaling processes.

Here we demonstrate that caging an agonist peptide with the NV-bound reliably allows its delivery through two-photon uncaging at the synaptic level. Moreover, we successfully demonstrated its use for the investigation of neuron-to-glia communication. In the neuroscience field, the role of every neural cell on the function and plasticity of neuronal network remains unclear and is the subject of intense investigation.[22] In this context, the ability to spatially and temporally deliver neurotransmitters or gliotransmitters through two-photon flash photolysis is undoubtedly a real asset. For this purpose and among others, glutamate, GABA, or dopamine could be caged with the two-photon-compatible NV-bound.

Two-photon uncaging is especially relevant as modern neuroscience studies commonly perform in vivo physiological investigations with the use of two-photon fluorescent microscopy, meaning that a growing amount of laboratories are equipped with the necessary tools. Interestingly, recent technical advancements in photostimulation techniques such as temporal and spatial light beam shaping permit delivery of patterned light with an excellent lateral and axial resolution even in deep tissue.[23] It has been recently successfully used for optogenetics based experiments.[24] Even if, to our knowledge, beam shaping has not been used for flash photolysis in vivo yet, it could help the precise delivery of a caged compound even within a complex cellular morphology such as dendritic arbor or astrocytic processes.

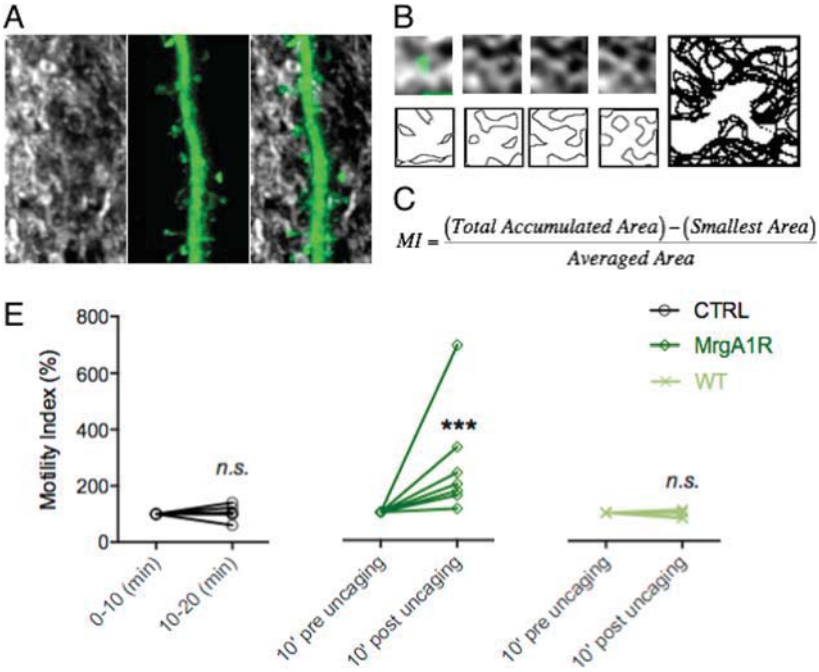

Figure 3. Two-photon uncaging of FMRFaNVTEG induces PAP movements at the synaptic level. (A) Confocal images of dendrites (green) and astrocytes (gray). (B) Top images show *Z*-stack projection of astrocytic processes (gray) around dendritic spine (green) monitored every 2 min. Bottom images show the outline of the projected astrocytic membrane. Right image represents the total accumulated outline of astrocytic membrane, highlighting the course of astrocytic process over a period of 20 min. (C) Motility index (MI) calculation formula. (D) MI index monitored in basal conditions for two consecutive 10 min periods (left graph, $n = 7$). Flash photolysis of FMRFa-NVTEG agonist peptide resulted in robust MI increase in infected astrocytes (middle graph, $n = 7$) but not in noninfected astrocytes (right graph, $n = 8$). (Data are Means ± SEM, Statistics are paired student *t* test, *n.s.* = $p > 0.05$; *** = $p < 0.001$).

FMRFa like other neuropeptides of the RFamide family are not expressed in central nerveous system (CNS) of adult vertebrates.[25] Interestingly, RFamide are only transiently expressed during the first stages of vertebrate development including in murines[26] and humans.[27] However, the exact role of endogenous RFamide during development is still unknown. The step-by-step synthesis procedure to inactivate FMRFa with a photocleavable bound described in the present study might be compatible with all RFamide and would undoubtedly provide an asset for this field of research. In turn, the precise control of RFa delivery through flash photolysis techniques could help understanding how exogenous application of RFamide could interfere with nociceptive signaling.[28]

EXPERIMENTAL SECTION

Material and Methods (adapted from ref 16). *Mice Organotypic Hippocampal Slice.* Organotypic hippocampal slice cultures were prepared as described previously.[29] Briefly, 400-μm-thick hippocampal slices were prepared from postnatal day 6−7 C57BL/6J mice and transferred onto culture membranes (Millipore, Billerica, MA, USA). Slices were cultured for 7−21 days in vitro in culture media.

DNA Cloning and Semliki Forest Virus Production. DNA of MrgA1 was obtained from Xinzhong Dong's laboratory[30] and cloned into SFV(A7) viral vector as described by us earlier.[16] Viral SFV(A7) particles were produced as described previously.[31]

Immunohistochemistry. Sixteen hours post infection, slices were fixed, blocked, and permeabilized following a standard procedure.[16] Slices were then incubated overnight at 4 °C with anti-GFAP or rabbit anti-S11B or anti-MycHis antibodies. The slices were mounted on slides for imaging.

Astrocytic Calcium Imaging. Ca^{2+} measurements in astrocytes were performed by bulk-loading of the Ca^{2+}-sensitive dye Fluo-8 (Teflabs). Dye was dissolved in DMSO containing 14% pluronic F127 (Sigma-Aldrich) to reach 2 mM. Dye bulk-loading was performed as described previously.[16] Loaded slices were placed on the stage of an upright microscope (BX51WI, Olympus) connected to a confocal spinning disk system (CSU10, Visitron System) and perfused with 34−35 °C ACSF. The ACSF solution contained (in mM): NaCl 130, KCl 3, $NaHCO_3$ 26, $CaCl_2$ 2, $MgCl_2$ 1.48, NaH_2PO_4 1.23, glucose 10, bubbled with 5% CO_2/95% oxygen. Fluo-8 was excited by a 488 nm laser diode (Oxxius) and emission collected through a 20× UMPlanFL N 0.5 N.A. water immersion objective (Olympus) to a charge-multiplying CCD camera (evolve 512, Photometrics). Single plane images were acquired at 1 Hz using Metafluor software (Molecular Devices). Fluorescence intensities were monitored and analyzed offline in cell soma using Metafluor. All Ca^{2+} increases above two standard deviations were collected. For success probability data, events occurring 0−10 s post-UV flash were considered as evoked by FMRFaNVTEG uncaging. One to three consecutive UV flashes were sent and the number of Ca^{2+} events per UV flash determined as percent.

Morphological Imaging. Imaging of PAP-spine interplay was performed as in our earlier work.[16] Briefly, viral gene delivery of farnesylated fluorescent proteins, eGFPf and mCherryf, was used to separately label astrocytic and neuronal membranes, respectively. Semliki Forest Viruses (SFV) having either a glial SFV(A7) or a neuronal SFV(PD) tropism were injected into mice hippocampal organotypic cultures. Time-lapse imaging was performed 12−24 h post virus injection with a laser scanning microscope (FV300, Olympus). *Z*-stacks of infected apical dendrites surrounded by infected astrocytic domain were monitored

sequentially using 0.6 μm z-steps. Z-stacks of spine-PAP pairs were acquired every 2 min during two consecutive 10 min periods. For quantification of PAP motility, an index of motility was computed offline (see Figure 3).

Flash Photolysis. Single- and two-photon flash photolysis were performed as in our earlier work.[16] For single photon, a high-power 365-nm LED was delivering light to astrocytes through an optical fiber equipped with a condenser. Astrocytes were photoactivated in the presence of FMRFaNVTEG in the extracellular bath (1−3 mM). 2P flash photolysis was achieved using repetitive 725 nm to 1.5 ms pulses (1 Hz, 8 pulses, laser power of 40−50 mW back focal plane).

General Synthetic Methods. Unless otherwise indicated, all reagents were obtained from commercial suppliers (Fluka, Aldrich, Acros, TCI, Iris) and were used without further purification. Deuterated solvents were obtained from Cambridge Isotope Laboratory. Analytical thin layer chromatography was performed on Kieselgel F-254 precoated aluminum sheets TLC plates from Merck. Visualization was performed with a 254 nm UV lamp and/or a $KMnO_4$ solution. Flash column chromatography (FC) was carried out using Brunschwig silica gel (SiO_2, 60 Å, 32−63 mesh) or reverse-phase silica gel (C18, 30 μm). ^{1}H NMR and ^{13}C NMR spectra were recorded on Bruker Avance DPX 360, Bruker-DRX-300, or Bruker Avance DPX 500 spectrometers. All NMR spectra were recorded in $CDCl_3$, CD_3CN, DMSO-d_6, D_2O, or CD_3COOD. Chemical shifts are expressed in parts per million (δ) using residual solvent protons as internal standards. Coupling constants (J) are reported in Hz. Splitting patterns are designated as s (singlet), d (doublet), dd (double doublet), t (triplet), dt (double triplet), q (quartet), bs (broad singlet), and m (multiplet). A PerkinElmer Lambda 40 UV/vis spectrometer was employed for the UV/vis spectra. Mass spectra at high resolution were recorded on a Bruker 4.7T BioApex II mass spectrometer. A Bruker Tensor 27 spectrometer equipped with a golden gate was used to record IR spectra. LC-MS was performed on an Aquity H-Class UPLC system equipped with an ESI-SQD mass spectrometer. Photoirradiations were performed with a Lumos 43 photoreactor (Atlas Photonics). The peptides were synthesized on a Syro I automated peptide synthesizer. Microwave assisted reactions were carried out with a Biotage Initiator, using sealable flasks. Photolyses were performed on a LED-based photoreactor (LUMOS 43, Atlas Photonics Inc.).

Synthesis of the Nitroveratrylamine 4. *4,5-Dimethoxy-2-nitrobenzyl-O-methyloxime (**3**).* A solution of 4,5-dimethoxy-2-nitrobenzaldehyde **2** (5 g, 23.68 mmol) and methoxyamine hydrochloride (1.978 g, 23.68 mmol) in 60 mL of a mixture of anhydrous ethanol and anhydrous pyridine 1:1 (v/v) was stirred at rt for 5 min. The solvents were evaporated. The residue was triturated in pentane/EtOAc 2:1 and filtered. **3** (5.7 g, 23.7 mmol, 96% yield) was obtained as a yellow solid. ^{1}H NMR (300 MHz, $CDCl_3$) δ 8.73 (s, 1 H), 7.63 (s, 1 H), 7.39 (s, 1 H), 4.04 (s, 3 H), 4.03 (s, 3 H), 3.98 (s, 3 H). ^{13}C NMR (75 MHz, $CDCl_3$) δ 153.1, 149.8, 145.6, 140.8, 122.0, 109.1, 107.5, 62.3, 56.5, 56.4. HRMS (ESI) for $C_{10}H_{12}N_2O_5$ ($M+Na^+$) calcd 263.0638, found 263.0643. FT-IR (golden gate, 600−4000 cm^{-1}) 3276, 3103, 2939, 2833, 1596, 1562, 1455, 1443, 1404, 1519, 1362, 1333, 1264, 1220, 1171, 1067, 1029, 992, 927, 873, 800, 754.

*4,5-Dimethoxy-2-nitrobenzylamine (**4**).* A solution of **3** (2.402 g, 10.00 mmol) in BH_3.THF 1 M (15 mL, 15.00 mmol) was stirred at rt for 2 h. 300 mL of water and 300 mL of KOH 20% were slowly added at 0 °C. The mixture was extracted with DCM. The organic layers were dried over Na_2SO_4 and concentrated under vacuum. The residue was purified by flash chromatography (RP18, MeCN/water 5%) to afford **4** (650 mg, 3.06 mmol, 31% yield) as a red oil. ^{1}H NMR (300 MHz, $CDCl_3$) δ 7.68 (s, 1 H), 7.07 (s, 1 H), 4.49 (bs, 2 H), 3.94−3.99 (m, 2 H), 3.93 (s, 3 H), 3.89 (s, 3 H). ^{13}C NMR (75 MHz, CD_3CN) δ 154.6, 150.0, 142.3, 127.1, 116.0, 109.4, 57.4, 57.1, 51.1. HR-MS (ESI) for $C_9H_{12}N_2O_4$ ($M+H^+$) calcd 213.0870, found 213.0873. FT-IR (golden gate, 600−4000 cm^{-1}) 3277, 2937, 1631, 1528, 1285, 1141, 1034, 735.

Synthesis of the Fmoc-Phe-Met-Arg(Pbf)-Phe-OH (5). The tetrapeptide was synthesized by Fmoc SPPS on an automated peptide synthesizer. Fmoc-L-amino acids from Iris Biotech were used. A Pbf (2,2,4,6,7-pentamethyldihydrobenzofuran-5-sulfonyl) protecting group was used for arginine. H-L-Phe-2-chlorotrytil resin (0.69 mmol/g, 6 vessels of 169 mg per synthesis) was used as first amino acid and was swollen in DMF. The amino acids (6 times 0.8 mL of a 0.5 M solution in DMF) were coupled onto the resin for 1 h using HCTU (6 times 0.84 mL of a 0.48 M solution in DMF) and *N,N*-diisopropylethylamine (6 times 0.4 mL of a 7% solution in NMP) as coupling agents. The resin was washed after each coupling three times with DMF (1 mL). The Fmoc protections were removed with piperidine (6 times 1.2 mL of a 40% solution in DMF) for 5 min. The resin was washed after each deprotection three times with DMF (1 mL). The peptide was removed from the resin with a solution of TFA, trifluoroethanol, and DCM (6 times 1.4 mL of a 1:1:8 solution) twice for 30 min. **5** (750 mg, 698 mmol, 99% yield) was obtained as a pale brown solid. ^{1}H NMR (300 MHz, Acetic acid-d_4) δ 7.77 (d, J = 7.5 Hz, 2 H), 7.46−7.61 (m, 2 H), 7.37 (t, J = 1.0 Hz, 2 H), 7.09−7.33 (m, 12 H), 4.88 (m, J = 8.2, 4.80 Hz, 1 H), 4.61 (m, J = 9.7, 4.60 Hz, 3 H), 4.32−4.44 (m, 1 H), 4.20−4.32 (m, 1 H), 4.07−4.20 (m, 1 H), 3.16−3.35 (m, 2 H), 2.88−3.20 (m, 6 H), 2.56 (s, 3 H), 2.50 (s, 3 H), 2.30−2.46 (m, 2 H), 2.06 (s, 3 H), 1.99 (s, 3 H), 1.87−1.97 (m, 2 H), 1.51−1.86 (m, 4 H), 1.45 (s, 6 H). ^{13}C NMR (75 MHz, Acetic acid-d_4) δ 176.1, 174.6, 173.8, 173.5, 163.9, 163.4, 157.6, 144.8, 142.3, 137.6, 137.4, 130.3, 129.5, 128.7, 128.1, 127.9, 127.8, 126.2, 126.1, 126.0, 120.9, 118.5, 87.6, 68.3, 57.3, 54.7, 53.8, 53.7, 48.0, 43.7, 38.7, 37.8, 32.2, 30.6, 30.1, 28.6, 18.2, 15.3, 12.6. HR-MS (ESI) for $C_{57}H_{67}N_7O_{10}S_2$ ($M+H^+$) calcd 1074.4464, found 1074.4465. FT-IR (golden gate, 600−4000 cm^{-1}) 3283, 2929, 1632, 1536, 1141, 664.

Synthesis of the FMRFaNV 7. *Phe-Met-Arg(Pbf)-Phe-NH-NV (**6**).* **5** (210 mg, 0.196 mmol) was dissolved in 2 mL of DMF. **4** (53 mg, 0.250 mmol) was added. HCTU (200 mg, 0.483 mmol), *N,N*-diisopropylethylamine (0.12 mL, 0.687 mmol), and NMP (Ratio: 0.1, Volume: 0.200 mL) were added and the mixture was stirred at room temperature for 10 min. Piperidine (4 mL, 40.4 mmol) was added and the mixture was stirred at room temperature for 2 h. The mixture was diluted with sodium hydrogenocarbonate and extracted with DCM. The collected organic layers were dried over Na_2SO_4 and concentrated under vacuum at room temperature. The residue was purified by flash chromatography (RP18, MeCN/water 20% → 100% in 17 column volumes). The collected fractions were concentrated, diluted with sodium hydrogenocarbonate, and extracted with DCM. The collected organic layers were dried over Na_2SO_4 and concentrated under vacuum at room temperature to afford **6** (80 mg, 0.077 mmol, 38% yield) as an orange solid. ^{1}H NMR (300 MHz, CD_3COOD) δ 7.66 (s, 1 H), 7.06−7.52 (m, 10 H), 7.02 (s, 1 H), 4.79−4.95 (m, 1 H), 4.57−4.70 (m, 3 H), 4.42−4.55 (m, 2 H), 3.92 (s, 6 H), 3.16−3.30 (m, 4 H), 3.02−3.10 (m, 2 H), 2.97 (bs., 2 H), 2.55 (s, 3 H), 2.49 (s, 3 H), 2.37−2.44 (m, 2 H), 2.07 (s, 3 H), 1.52−1.98 (m, 9 H), 1.38−1.49 (m, 6 H). ^{13}C NMR (75 MHz, CD_3COOD) δ 173.7, 173.5, 173.0, 169.9, 166.3,

160.2, 157.6, 154.8, 149.4, 141.4, 139.8, 137.1, 134.6, 130.6, 130.2, 129.9, 129.4, 128.8, 128.7, 127.9, 126.1, 118.6, 114.2, 109.2, 87.7, 56.9, 56.6, 56.0, 54.0, 49.8, 48.8, 43.7, 42.4, 40.6, 37.8, 30.4, 28.6, 26.5, 25.3, 18.2, 15.2, 12.6. HR-MS (ESI) for $C_{51}H_{67}N_9O_{11}S_2$ ($M+H^+$) calcd 1046.4474, found 1046.4482. FT-IR (golden gate, 600−4000 cm^{-1}) 3296, 2932, 1635, 1518, 1273, 1103, 729.

*Phe-Met-Arg-Phe-NH-NV (**7**).* **6** (80 mg, 0.077 mmol) was stirred in TFA (10 mL, 130 mmol) and 0.5 mL of water for 45 min at room temperature. The mixture was neutralized with sodium hydrogenocarbonate and extracted with DCM. The collected organic layers were dried over Na_2SO_4 and concentrated under vacuum at room temperature. The residue was purified by flash chromatography (RP18, MeCN/H_2O 30% → 100% in 10 column volumes). The collected fractions were concentrated, diluted with sodium hydrogenocarbonate, and extracted with DCM. The collected organic layers were dried over Na_2SO_4 and concentrated under vacuum at room temperature to afford **7** (50 mg, 0.063 mmol, 82% yield) as a yellow solid. ^{1}H NMR (500 MHz, Acetic acid-d_4) δ 7.67 (s, 1 H), 7.23−7.32 (m, 5 H), 7.14−7.18 (m, 3 H), 7.07−7.12 (m, 2 H), 7.02 (s, 1 H), 4.88 (dd, J = 7.8, 6.90 Hz, 1 H), 4.7 (d, J = 8.0 Hz, 2 H), 4.6 (dd, J = 8.6, 5.43 Hz, 1 H), 4.49−4.55 (m, 2 H), 3.94 (s, 3 H), 3.92 (s, 3 H), 3.15−3.30 (m, 4 H), 3.00 (m, J = 14.0, 8.00 Hz, 2 H), 2.38−2.49 (m, 2 H), 1.86−1.95 (m, 2 H), 1.71−1.84 (m, 2 H), 1.59−1.67 (m, 2 H). ^{13}C NMR (126 MHz, Acetic acid-d_4) δ 180.1, 173.7, 173.6, 173.3, 154.8, 149.4, 141.4, 137.1, 130.6, 130.2, 129.9, 129.4, 128.7, 127.9, 114.1, 109.3, 71.1, 56.9, 56.7, 55.9, 54.3, 54.1, 42.4, 41.7, 38.8, 37.9, 32.3, 30.6, 30.3, 25.7, 23.5, 15.2. HR-MS (ESI) for $C_{38}H_{51}N_9O_8S$ ($M+H^+$) calcd 794.3654, found 794.3650. FT-IR (golden gate, 600−4000 cm^{-1}) 3317, 2933, 1648, 1518, 1272, 700.

Photolysis Test. **7** (10 mg, 0.013 mmol) was diluted in 1 mL of MeCN and irradiated at 385 nm with a Lumos 43 photoreactor (Atlas Photonics) in a quartz absorption cell (1 cm width) for 3 h. UPLC-MS analysis showed formation of **1**, together with small amount of unreacted **7**. MS (ESI) for $C_{29}H_{42}N_8O_4S$ ($M-H^+$) calcd 599.3123, found 599.3.

Synthesis of the TEGNVNH$_2$ 16. *4-(Benzyloxy)-3-methoxybenzaldehyde (**9**).* **8** (4.05 g, 26.6 mmol) was dissolved in 60 mL of acetone. Benzyl bromide (3.17 mL, 26.6 mmol) and potassium carbonate (1.839 g, 13.31 mmol) were added and the mixture was heated at reflux for 16 h, then diluted with sodium hydrogenocarbonate and extracted with DCM. The collected organic phases were washed with sodium hydrogenocarbonate, dried over $MgSO_4$, and concentrated under vacuum. **9** (6.348 g, 26.2 mmol, 98% yield) was obtained as a yellow oil. ^{1}H NMR (300 MHz, $CDCl_3$) δ 9.85 (s, 1 H), 7.28−7.50 (m, 7 H), 7.00 (d, J = 8.1 Hz, 1 H), 5.26 (s, 2 H), 3.96 (s, 3 H). Additional data reported elsewhere.[32]

*4-(Benzyloxy)-5-methoxy-2-nitrobenzaldehyde (**10**).* A solution of **9** (1.557 g, 6.43 mmol) in nitric acid (60%, 7.5 mL, 168 mmol) was stirred at room temperature for 1 h, then concentrated and recrystallized in EtOAc to give **10** (768 mg, 2.67 mmol, 42% yield) as yellow crystals. ^{1}H NMR (360 MHz, $CDCl_3$) δ 10.45 (s, 1 H), 7.68 (s, 1 H), 7.31−7.54 (m, 6 H), 5.29 (s, 2 H), 4.03 (s, 3 H). Additional data reported elsewhere.[33]

*4-Hydroxy-5-methoxy-2-nitrobenzaldehyde (**11**).* A solution of **10** (676 mg, 2.353 mmol) in acetic acid (10 mL) was warmed up to 80 °C. Hydrobromic acid (48% in water, 1.331 mL, 11.77 mmol) was added and the mixture was heated in a sealed flask in a microwave oven at 90 °C for 1 h 30 min. The precipitate was filtered off and the residue was dried under high vacuum. **11** (311 mg, 1.58 mmol, 67% yield) was obtained as yellow crystals. ^{1}H NMR (360 MHz, $CDCl_3$) δ 10.41 (s, 1 H), 7.69 (s, 1 H), 7.47 (s, 1 H), 6.23 (bs., 1 H), 4.08 (s, 3 H). Additional data reported elsewhere.[32]

*2-{2-[2-(2-Hydroxyethoxy)ethoxy]ethoxy}ethyl 4-methylbenzenesulfonate (**13**).* A solution of sodium hydroxide (0.695 g, 17.38 mmol) in 3 mL of water was added to a solution of tetraethylene glycol **12** (20 mL, 116 mmol) in 3 mL of THF and cooled down to 0 °C. Tosyl chloride (2.209 g, 11.58 mmol) in 10 mL of THF was added slowly and the mixture stirred at 0 °C for 1 h and at rt for 2 h. The mixture was extracted with DCM. The collected organic layers were dried over $MgSO_4$, filtered, and concentrated under vacuum to afford **13** (4.01 g, 11.50 mmol, 99% yield) as a yellowish oil. ^{1}H NMR (360 MHz, $CDCl_3$) δ 7.80 (d, J = 8.2 Hz, 2 H), 7.35 (d, J = 7.7 Hz, 2 H), 4.16 (t, J = 4.5 Hz, 2 H), 3.51−3.84 (m, 15 H), 2.45 (s, 3 H). The ^{1}H NMR spectrum suggested the presence of tetraethylene glycol impurities. Additional data reported elsewhere.[34]

*4-{2-[2-(2-Hydroxyethoxy)ethoxy]ethoxy}ethoxy-5-methoxy-2-nitrobenzaldehyde (**14**).* Anhydrous potassium carbonate (386 mg, 2.79 mmol) was added to a solution of **13** (972 mg, 2.79 mmol) in 10 mL of dry THF. The mixture was stirred at rt for 10 min; then **11** (500 mg, 2.54 mmol) was added and the mixture heated in a microwave oven at 100 °C for 3 h, then diluted with water, basified with NaOH 1 M, and extracted with DCM. The aqueous layer was acidified with HCl 1 N and extracted again with DCM. The collected organic layers were washed with NaOH 1M, dried over $MgSO_4$, filtered, and concentrated under vacuum to afford **14** (928 mg, 2.49 mmol, 98% yield) as an orange oil. ^{1}H NMR (300 MHz, CD_3CN) δ 10.26 (s, 1 H), 7.66 (s, 1 H), 7.37 (s, 1 H), 4.28 (t, J = 1.0 Hz, 2 H), 3.97 (s, 3 H), 3.83 (m, J = 5.3 Hz, 2 H), 3.61−3.68 (m, 2 H), 3.51−3.61 (m, 9 H), 3.40−3.51 (m, 2 H). ^{13}C NMR (75 MHz, CD_3CN) δ 189.2, 154.4, 152.7, 144.9, 126.4, 111.0, 109.6, 73.4, 71.5, 71.3, 71.2, 71.1, 70.3, 69.9, 62.0, 57.4. HR-MS (ESI) for $C_{16}H_{23}NO_9$ ($M+Na^+$) calcd 396.1265, found 396.1269. FT-IR (golden gate, 600−4000 cm^{-1}) 3469, 2871, 1688, 1601, 1572, 1519, 1460, 1339, 1331, 1282, 1222, 1060, 875, 802, 736.

*4-{2-[2-(2-Hydroxyethoxy)ethoxy]ethoxy}ethoxy-5-methoxy-2-nitrobenzyl-O-methyloxime (**15**).*[18] A solution of **14** (1.343 g, 3.60 mmol) and methoxyamine hydrochloride (0.300 g, 3.60 mmol) in 20 mL of a mixture of anhydrous methanol and dry pyridine 1:1 was stirred at rt for 2 min. The solvents were evaporated; the residue was diluted with water and extracted with DCM. The collected organic layers were dried over Na_2SO_4, filtered, and concentrated under vacuum. **15** (1.423 mg, 3.54 mmol, 98% yield) was obtained as an orange oil. ^{1}H NMR (300 MHz, CD_3CN) δ 8.52 (s, 1 H), 7.65 (s, 1 H), 7.35 (s, 1 H), 4.21 (m, J = 4.5 Hz, 2 H), 3.97 (s, 3 H), 3.95 (s, 3 H), 3.77−3.85 (m, 2 H), 3.61−3.66 (m, 2 H), 3.51−3.61 (m, 9 H), 3.48 (m, J = 4.9 Hz, 2 H). ^{13}C NMR (75 MHz, CD_3CN) δ 154.5, 150.3, 146.7, 142.0, 122.6, 110.5, 110.0, 73.4, 71.5, 71.3, 71.2, 71.1, 69.9, 70.0, 62.9, 62.0, 57.2. HR-MS (ESI) for $C_{17}H_{26}N_2O_9$ ($M+Na^+$) calcd 425.1531, found 425.1532. FT-IR (golden gate, 600−4000 cm^{-1}) 3444, 2937, 2873, 1601, 1564, 1333, 1280, 1220, 1076.

*4-{2-[2-(2-Hydroxyethoxy)ethoxy]ethoxy}ethoxy-5-methoxy-2-nitrobenzylamine (**16**).*[33] To **15** (1.540 g, 3.83 mmol) at 0 °C was slowly added BH_3.THF (30 mL, 30.0 mmol). The solution was stirred at 0 °C for 5 min and then heated at reflux for 2 h. The mixture was cooled to 0 °C and 20 mL of H_2O and 20 mL of KOH 20% were slowly added at 0 °C. The mixture was basified to pH 11−12 with conc. NaOH and extracted with DCM. The collected organic layers were dried over Na_2SO_4,

filtered and concentrated under vacuum. FC (RP18, MeCN 100%) afforded **16** (1.358 g, 3.63 mmol, 95% yield) as an orange oil. The free amine is not stable and must be kept at −20 °C under argon. To increase its stability, the amine can be obtained as its hydrochloric salt by extraction with HCl 1 N and concentration of the aqueous phase under vacuum at 50 °C. A more stable dark red oil was obtained. ^{1}H NMR (300 MHz, D_2O) δ 7.80 (s, 1 H), 7.14 (s, 1 H), 4.31−4.37 (m, 2 H), 4.21−4.28 (m, 2 H), 3.92 (s, 3 H), 3.84−3.90 (m, 2 H), 3.66−3.72 (m, 2 H), 3.57−3.66 (m, 8 H), 3.50−3.56 (m, 2 H). ^{13}C NMR (75 MHz, CD_3COOD) δ 153.2, 147.6, 140.5, 122.3, 114.8, 109.8, 71.3, 69.4, 69.3, 69.2, 69.0, 68.3, 68.1, 59.9, 56.2, 40.9. HR-MS (ESI) for $C_{16}H_{26}N_2O_8$ ($M+H^+$) calcd 375.1762, found 375.1755. FT-IR (golden gate, 600−4000 cm^{-1}) 2870, 2362, 1676, 1580, 1522, 1459, 1334, 1279, 1220, 1101, 1065, 946.

Synthesis of the FMRFaNVTEG 18. *Phe-Met-Arg(Pbf)-Phe-NH-NV-TEG (17).* **5** was dissolved in 1 mL of DMF. **16** (444 mg, 1.187 mmol) was added. NMP (Ratio: 0.1, Volume: 0.050 mL), HCTU (1309 mg, 3.16 mmol), and *N,N*-diisopropylethylamine (0.553 mL, 3.16 mmol) were added and the mixture was stirred at rt for 1 h 30 min. Piperidine (15 mL, 152 mmol) was added and the mixture was stirred at rt for 5 min, then diluted with sodium hydrogenocarbonate and extracted with DCM. The collected organic layers were dried over Na_2SO_4, filtered, and concentrated under vacuum at rt. The residue was purified by FC (RP18, MeCN/H_2O 30% → 100%). The collected fractions were concentrated, diluted with sodium hydrogenocarbonate, and extracted with DCM. The collected organic layers were dried over Na_2SO_4, filtered, and concentrated under vacuum at rt to afford **17** (140 mg, 0.375 mmol, 47.4% yield) as a yellowish solid. ^{1}H NMR (300 MHz, CD_3CN) δ 8.12 (bs., 1 H), 7.61−7.69 (m, 1 H), 7.57 (bs, 1 H), 7.41 (bs., 1 H), 7.04−7.31 (m, 10 H), 7.01 (s, 1 H), 6.19 (bs, 2 H), 5.16 (bs, 4 H), 4.61 (s, 2 H), 4.16−4.51 (m, 4 H), 4.13 (bs, 2 H), 3.83 (s, 3 H), 3.69−3.81 (m, 2 H), 3.42−3.66 (m, 12 H), 3.11 (s, 6 H), 2.89−2.95 (m, 2 H), 2.51 (bs, 3 H), 2.44 (bs, 3 H), 2.27−2.40 (m, 2 H), 2.01 (s, 3 H), 1.97 (s, 3 H), 1.44−1.89 (m, 6 H), 1.39 (s, 6 H). ^{13}C NMR (75 MHz, CD_3COOD) δ 172.8, 172.7, 172.1, 169.6, 165.6, 159.5, 157.7, 154.7, 147.7, 141.2, 139.1, 138.1, 135.1, 134.3, 133.3, 130.6, 130.3, 130.3, 130,0, 129.4, 128.8, 127.8, 126.1, 113.3, 110.8, 87.7, 72.9, 71.1, 70.8, 70.7, 70.6, 69.9, 69.7, 61.8, 57.6, 56.1, 55.8, 54.3, 53.9, 48.6, 43.6, 41.8, 38.4, 38.2, 32.4, 30.6, 28.8, 26.6, 25.5, 19.75, 18.5, 15.5, 12.8. HR-MS (ESI) for $C_{58}H_{81}N_9O_{15}S_2$ ($M+H^+$) calcd 1208.5366, found 1208.5360. FT-IR (golden gate, 600−4000 cm^{-1}) 2935, 1643, 1519, 1274, 1090, 837, 643.

Phe-Met-Arg-Phe-NH-NV-TEG (18). **17** (115 mg, 0.095 mmol) was stirred in TFA (10 mL, 130 mmol) and 0.5 mL of water for 1 h at rt. The mixture was basified with sodium hydrogenocarbonate and extracted with DCM. The collected organic layers were dried over Na_2SO_4, filtered, and concentrated under vacuum at rt. The residue was purified by FC (RP18, MeCN/H_2O 30% → 100%). The collected fractions were concentrated, diluted with sodium hydrogenocarbonate, and extracted with DCM. The collected organic layers were dried over Na_2SO_4, filtered, and concentrated under vacuum at rt to afford **18** (75 mg, 0.078 mmol, 82% yield) as a yellow oil. ^{1}H NMR (300 MHz, CD_3COOD) δ 7.73 (s, 1 H), 7.07−7.38 (m, 10 H), 7.04 (s, 1 H), 4.89 (t, J = 7.4 Hz, 1 H), 4.55−4.63 (m, 1 H), 4.46−4.54 (m, 2 H), 4.22−4.31 (m, 2 H), 3.88−3.99 (m, 5 H), 3.67−3.82 (m, 12 H), 3.64 (m, J = 4.9 Hz, 2 H), 2.94−3.31 (m, 6 H), 2.30−2.52 (m, 2 H), 2.03 (s, 3 H), 1.86−1.99 (m, 2 H), 1.72−1.86 (m, 2 H), 1.51−1.69 (m, 2 H). ^{13}C NMR (75 MHz, CD_3COOD) δ 173.6, 173.5, 173.1, 169.9, 157.9, 154.9, 148.3, 141.2, 137.1, 134.9, 130.5, 130.1, 129.8, 129.3, 129.1, 128.6, 127.8, 117.9, 114.0, 110.7, 72.8, 71.3, 71.0, 70.8, 70.2, 69.6, 61.7, 56.9, 55.8, 55.7, 54.2, 53.8, 42.2, 41.6, 38.6, 37.8, 32.3, 30.4, 25.6, 15.1. HR-MS (ESI) for $C_{45}H_{65}N_9O_{12}S$ ($M+H^+$) calcd 956.4546, found 956.4542. FT-IR (golden gate, 600−4000 cm^{-1}) 2925, 2361, 2342, 1709, 1663, 1520, 1399, 1273, 1067, 1033, 924, 832.

Photolysis Test. 18 (ca 1 mg) was dissolved in 0.7 mL of D_2O and irradiated at 385 nm with a Lumos 43 photoreactor (Atlas Photonics) in a regular NMR tube for 20 min. HRMS and NMR analysis showed, complete disappearance of **18**, and the formation of **1**. MS (ESI) for $C_{29}H_{42}N_8O_4S$ ($M+H^+$) calcd 599.3123, found 599.3124. NMR analysis of the crude mixture in D_2O showed the liberation of FMRFa, by overlay with an authentic sample (SI, page S56).

Quantum Yield Measurement. *General Procedure for Ferrioxalate Actinometry.*[35] General remarks: The value of the quantum flow of a lamp is only valid for a precise position in the optical path and for the same photochemical reactor and absorption cell. The solution has to absorb all the light during the whole irradiation time. At excitation wavelengths below 380 nm, 0.006 M ferrioxalate solution is used. For wavelengths between 380 and 450 nm, a 0.15 M solution is used. All processing steps have to be executed in the darkness.

Preparation of the Solutions.

(A) 147.5 mg (for 0.006 M solution) or 3.69 g (for 0.15 M solution) of potassium ferrioxalate is completely dissolved in 40 mL of water by ultrasonication. 5 mL of 1 N sulfuric acid is added and the solution is then diluted to 50 mL. **Caution: Prepare and store the solution in the dark!**

(B) 50 mg of *o*-phenanthroline is dissolved in 50 mL of water.

(C) 3.4 g of sodium acetate trihydrate is dissolved in 25 mL of water. 15 mL of this solution is mixed with 9 mL of 1 N sulfuric acid and diluted to 25 mL (buffer solution at pH 3.5).

Measurement. The lamp is switched on and left to equilibrate for 30 min to be sure that the temperature in the reactor is stable. 3 mL (V_1) of the ferrioxalate−solution A is pipetted into the absorption cell (1 cm width) and irradiated. 2 mL (V_2) of the irradiated solution is mixed with 2 mL phenanthroline-solution B and 1 mL buffer solution C in a 20 mL graduated flask and diluted to 20 mL (V_3). 2 mL of the nonirradiated solution A is treated exactly the same way and both solutions are stored for 1 h in absolute darkness. The optical density of both solutions is measured at 510 nm. The nonirradiated solution serves as reference solution. Several irradiations using different irradiation times are performed.

Calculation of the Quantum Flow. The optical density (D) is plotted as a function of the time. The resulting graph should be a straight line through the zero point. A flattening of the graph at longer irradiation time indicates a bleaching of the actinometer-solution. The slope (D/t) is determined only with those points that are lying on the straight line.

The amount of photons (Einstein) entering the cell per second is calculated using the following equation:

$$\text{Quantum flow[Einstein/s]} = \frac{D \cdot V_1 \cdot V_3}{t \cdot \phi \cdot \varepsilon \cdot d \cdot V_2}$$

D = optical density of the irradiated solution at 510 nm	V_1 = irradiated volume (3 mL)
t = irradiation time in seconds	V_2 = used volume of V_1 (2 mL)
ϕ = quantum yield at the irradiation wavelength	V_3 = end volume (20 mL)
ε = extinction coefficient of the complex at 510 nm (1.11 × 10^4 L/mol/cm)	d = cell thickness cell (1 cm)

The number of moles of photons emitted by the lamp can be calculated and plotted as a function of the time. The slope indicates the quantum flow of the lamp.

Quantum Flow of the 360 nm Lamp of the Lumos 43. The ferrioxalate solutions were prepared following the general procedure for the ferrioxalate actinometry and irradiated during 30 s and 1, 2, 4, and 6 min using the 360 nm lamp, then complexated with the phenantroline. A UV/vis absorbance spectrum was recorded for each solution. Using the optical density at 510 nm and the equation described in the general procedure (ϕ at 360 nm = 1.26), the amount of photons entering the cell was calculated and plotted as a function of the time. A value of 1.33×10^{-8} E/s or 4.79×10^{-5} E/h was obtained as quantum flow of the 360 nm LED lamp of the Lumos 43.

Quantum Yield of the FMRFaNVTEG. A 0.4 mM solution of FMRFaNVTEG **17** in water was prepared ($A = 0.726$). 3 mL of the solution was put in a standard absorbance cell (1 cm width) and irradiated in the photoreactor Lumos 43 for a given time. A UV/vis absorbance spectrum was recorded. The procedure of irradiation and analysis was repeated several times. Disappearance of the starting product (absorbance values at 350 nm) was plotted as a function of the time. To determine the rate of photolysis the linear regression of the first part of the plot was used. The slope being linear, it can be considered that the photolysis was a zero order reaction. The function of the trend line was used to determine the time needed to achieve the reference absorbance, which is the absorbance of the products of photolysis ($t > 50$ h, $A = 0.345$). The obtained rate value was then divided by the previously measured quantum flow, adapted following the Beer–Lambert law, because the solution has an absorbance value of 0.726, and consequently it does not absorb all the photons. A quantum yield of 0.023 was finally obtained.

■ ASSOCIATED CONTENT

Supporting Information

The Supporting Information is available

Spectra (^{1}H NMR, ^{13}C NMR, IR, HRMS) for all new substances (PDF)

■ AUTHOR INFORMATION

Corresponding Author

*E-mail: christian.bochet@unifr.ch.

Notes

The authors declare no competing financial interest.

[#]Deceased on April 29, 2015.

■ ACKNOWLEDGMENTS

The generous support of the Swiss National Science Foundation (grant 200020-1129617 to C.B.) and FP7-IIF-Marie Curie no 254022 to Y.B. and D.M. are gratefully acknowledged.

■ REFERENCES

(1) Kettenmann, H., and Ransom, B. R. (2005) *Neuroglia*, Oxford University Press, Oxford.

(2) Halassa, M. M., Fellin, T., and Haydon, P. G. (2007) The tripartite synapse: roles for gliotransmission in health and disease. *Trends Mol. Med. 13*, 54–63.

(3) Danbolt, N. C. (2001) Glutamate uptake. *Prog. Neurobiol. 65*, 1–105.

(4) Magistretti, P. J., Pellerin, L., Rothman, D. L., and Shulman, R. G. (1999) Energy on Demand. *Science 283*, 496–497.

(5) Allaman, I., Bélanger, M., and Magistretti, P. J. (2011) Astrocyte–neuron metabolic relationships: for better and for worse. *Trends Neurosci. 34*, 76–87.

(6) Benfenati, V., and Ferroni, S. (2010) Water transport between CNS compartments: functional and molecular interactions between aquaporins and ion channels. *Neuroscience 168*, 926–940.

(7) Ventura, R., and Harris, K. M. (1999) Three-Dimensional Relationships between Hippocampal Synapses and Astrocytes. *J. Neurosci. 19*, 6897–6906.

(8) Lavialle, M., Aumann, G., Anlauf, E., Pröls, F., Arpin, M., and Derouiche, A. (2011) Structural plasticity of perisynaptic astrocyte processes involves ezrin and metabotropic glutamate receptors. *Proc. Natl. Acad. Sci. U. S. A. 108*, 12915–12919.

(9) Agulhon, C., Fiacco, T. A., and McCarthy, K. D. (2010) Hippocampal Short- and Long-Term Plasticity Are Not Modulated by Astrocyte Ca2+ Signaling. *Science 327*, 1250–1254.

(10) Petreanu, L., Huber, D., Sobczyk, A., and Svoboda, K. (2007) Channelrhodopsin-2-assisted circuit mapping of long-range callosal projections. *Nat. Neurosci. 10*, 663–668.

(11) Fiacco, T. A., Agulhon, C., Taves, S. R., Petravicz, J., Casper, K. B., Dong, X., Chen, J., and McCarthy, K. D. (2007) Selective Stimulation of Astrocyte Calcium In Situ Does Not Affect Neuronal Excitatory Synaptic Activity. *Neuron 54*, 611–626.

(12) Cornell-Bell, A., Finkbeiner, S., Cooper, M., and Smith, S. (1990) Glutamate induces calcium waves in cultured astrocytes: long-range glial signaling. *Science 247*, 470–473.

(13) Volterra, A., and Meldolesi, J. (2005) Astrocytes, from brain glue to communication elements: the revolution continues. *Nat. Rev. Neurosci. 6*, 626–640.

(14) Ehrengruber, M. U., Renggli, M., Raineteau, O., Hennou, S., Vähä-Koskela, M. J., Hinkkanen, A. E., and Lundstrom, K. (2003) Semliki Forest Virus A7(74) Transduces Hippocampal Neurons and Glial Cells in a Temperature-Dependent Dual Manner. *J. NeuroVirol. 9*, 16–28.

(15) Haber, M., Vautrin, S., Fry, E. J., and Murai, K. K. (2009) Subtype-specific oligodendrocyte dynamics in organotypic culture. *Glia 57*, 1000–1013.

(16) Bernardinelli, Y., Randall, J., Janett, E., Nikonenko, I., König, S., Jones, E. V., Flores, C. E., Murai, K. K., Bochet, C. G., Holtmaat, A., et al. (2014) Activity-Dependent Structural Plasticity of Perisynaptic Astrocytic Domains Promotes Excitatory Synapse Stability. *Curr. Biol. 24*, 1679–1688.

(17) Klán, P., Šolomek, T., Bochet, C. G., Blanc, A., Givens, R., Rubina, M., Popik, V., Kostikov, A., and Wirz, J. (2013) Photoremovable protecting groups in chemistry and biology: reaction mechanisms and efficacy. *Chem. Rev. 113*, 119–191.

(18) Salerno, C. P., Resat, M., and Magde, D. (1997) Synthesis of Caged NAD (P)+ Coenzymes: Photorelease of NADP. *J. Am. Chem. Soc. 119*, 3403–3404.

(19) Veronese, F. M., and Harris, J. M. (2002) Introduction and overview of peptide and protein pegylation. *Adv. Drug Delivery Rev. 54*, 453–456.

(20) Tsai, S.-C., and Klinman, J. P. (2003) De Novo design and utilization of photolabile caged substrates as probes of hydrogen tunneling with horse liver alcohol dehydrogenase at sub-zero temperatures: a cautionary note. *Bioorg. Chem. 31*, 172–190.

(21) Šolomek, T., Mercier, S., Bally, T., and Bochet, C. G. (2012) Photolysis of ortho-nitrobenzylic derivatives: the importance of the leaving group. *Photochem. Photobiol. Sci. 11*, 548.

(22) Bernardinelli, Y., Muller, D., and Nikonenko, I. (2014) Astrocyte-Synapse Structural Plasticity. *Neural Plast. 2014*, 1–13.

(23) Zhu, G., van Howe, J., Durst, M., Zipfel, W., and Xu, C. (2005) Simultaneous spatial and temporal focusing of femtosecond pulses. *Opt. Express 13*, 2153–2159.

(24) Rickgauer, J. P., Deisseroth, K., and Tank, D. W. (2014) Simultaneous cellular-resolution optical perturbation and imaging of place cell firing fields. *Nat. Neurosci. 17*, 1816–1824.

(25) Sandvik, G. K., Hodne, K., Haug, T. M., Okubo, K., and Weltzien, F.-A. (2014) RFamide Peptides in Early Vertebrate Development. *Front. Endocrinol. 5*, 203.

(26) (a) Yano, T., Iijima, N., Kakihara, K., Hinuma, S., Tanaka, M., and Ibata, Y. (2003) Localization and neuronal response of RFamide related peptides in the rat central nervous system. *Brain Res. 982*, 156−167. (b) Attila, M., Kurkijarvi, U., Kivipelto, L., Panula, P., and Ahtee, L. (1995) The antiopioid peptide, neuropeptide FF, enhances the effects of acute morphine on the cerebral monoamines in rats. *Pharmacol. Res. 32*, 293−298.

(27) Bruzzone, F., Lectez, B., Tollemer, H., Leprince, J., Dujardin, C., Rachidi, W., Chatenet, D., Baroncini, M., Beauvillain, J.-C., Vallarino, M., et al. (2006) Anatomical distribution and biochemical characterization of the novel RFamide peptide 26RFa in the human hypothalamus and spinal cord. *J. Neurochem. 99*, 616−627.

(28) (a) Yudin, Y. K., Tamarova, Z. A., Ostrovskaya, O. I., Moroz, L. L., and Krishtal, O. A. (2004) RFa-related peptides are algogenic: evidence in vitro and in vivo. *Eur. J. Neurosci. 20*, 1419−1423. (b) Ugawa, S., Ueda, T., Ishida, Y., Nishigaki, M., Shibata, Y., and Shimada, S. (2002) Amiloride-blockable acid-sensing ion channels are leading acid sensors expressed in human nociceptors. *J. Clin. Invest. 110*, 1185−1190.

(29) De Roo, M., Klauser, P., and Muller, D. (2008) LTP Promotes a Selective Long-Term Stabilization and Clustering of Dendritic Spines. *PLoS Biol. 6*, e219.

(30) Han, S. K., Dong, X., Hwang, J. I., Zylka, M. J., Anderson, D. J., and Simon, M. I. (2002) Orphan G protein-coupled receptors MrgA1 and MrgC11 are distinctively activated by RF-amide-related peptides through the G q/11 pathway. *Proc. Natl. Acad. Sci. U. S. A. 99*, 14740−14745.

(31) Haber, M., Zhou, L., and Murai, K. K. (2006) Cooperative Astrocyte and Dendritic Spine Dynamics at Hippocampal Excitatory Synapses. *J. Neurosci. 26*, 8881−8891.

(32) Tsai, S.-C., and Klinman, J. P. (2003) De Novo design and utilization of photolabile caged substrates as probes of hydrogen tunneling with horse liver alcohol dehydrogenase at sub-zero temperatures: a cautionary note. *Bioorg. Chem. 31*, 172−190.

(33) Shirude, P. S., Kumar, V. A., and Ganesh, K. N. (2005) BisPNA Targeting to DNA: Effect of Neutral Loop on DNA Duplex Strand Invasion byaepPNA-N7G/aepPNA-C Substituted Peptide Nucleic Acids. *Eur. J. Org. Chem. 2005*, 5207−5215.

(34) Kimura, M., Kajita, K., Onoda, N., and Morosawa, S. (1990) The development of a new nitrating agent: the unusual regioselective nitration of diphenylpolyethylene glycols and phenylpolyethylene glycols with (trimethylsilyl) nitrate-BF3OEt2. *J. Org. Chem. 55*, 4887−4892.

(35) Montalti, M., Credi, A., Prodi, L., and Gandolfi, M. T. (2006) *Handbook of Photochemistry*, 3rd ed., Taylor and Francis, Boca Raton.